

Spatial Structure Design of Thioether-Linked Naphthoquinone Cathodes for High-Performance Aqueous Zinc–Organic Batteries

Qi-Qi Sun, Jia-Yi Du, Tao Sun, Zhen-Bang Zhuang, Zi-Long Xie, Hai-Ming Xie,* Gang Huang,* and Xin-Bo Zhang*

Organic electrode materials (OEMs) have gathered extensive attention for aqueous zinc-ion batteries (AZIBs) due to their structural diversity and molecular designability. However, the reported research mainly focuses on the design of the planar configuration of OEMs and does not take into account the important influence of the spatial structure on the electrochemical properties, which seriously hamper the further performance liberation of OEMs. Herein, this work has designed a series of thioether-linked naphthoquinone-derived isomers with tunable spatial structures and applied them as the cathodes in AZIBs. The incomplete conjugated structure of the elaborately engineered isomers can guarantee the independence of the redox reaction of active groups, which contributes to the full utilization of active sites and high redox reversibility. In addition, the position isomerization of naphthoquinones on the benzene rings changes the zincophilic activity and redox kinetics of the isomers, signifying the importance of spatial structure on the electrochemical performance. As a result, the 2,2'-(1,4-phenylenedithio) bis(1,4-naphthoquinone) (*p*-PNQ) with the smallest steric hindrance and the most independent redox of active sites exhibits a high specific capacity (279 mAh g⁻¹), an outstanding rate capability (167 mAh g⁻¹ at 100 A g⁻¹), and a long-term cycling lifetime (over 2800 h at 0.05 A g⁻¹).

1. Introduction

Low-carbon economy and sustainable development have gradually become the consensus in responding to the current energy and environment crisis. This requires us to vigorously develop renewable energy and increase the occupation of renewable energy in coal, petroleum, and natural gas-based power generation and transportation areas, so as to reduce our dependence on traditional energy sources. However, the uneven and intermittent distribution of renewable energy sources, such as solar and wind powers, requires us to find suitable energy storage technology to meet the needs of our daily lives. Among the available battery systems, aqueous zinc-ion batteries (AZIBs) are considered to be a competitive candidate for the new generation of energy storage systems owing to the high specific capacity (820 mAh g⁻¹) and suitable redox potential (−0.762 V versus SHE) of Zn anode, as well as the high safety and low cost of aqueous

electrolyte.^[1–4] Especially, considering that the organic electrode materials (OEMs) are composed of naturally abundant elements (C, O, H, N) and possess flexible structures and special coordination reaction mechanism for the storage/release of Zn²⁺,^[5–9] the construction of aqueous zinc-organic batteries is more competitive for large-scale energy storage. At present, the research of OEMs mainly focuses on developing new molecules or improving the performance based on existing organic materials. As for the brand-new organic molecules, inhibiting their dissolution in the electrolyte is generally considered to be the first prerequisite for obtaining excellent electrochemical performance. Researchers usually improve the stability of OEMs by designing extended π -conjugated structures or polymerizing to enlarge the active molecules. For example, Sun et al. reported a small organic molecule benzo[*i*]benzo[6',7']quinoxalino[2',3':9,10]phenanthro[4,5-*abc*]phenazine-5,10,16,21-tetraone (PTONQ) with an extended π -conjugated plane structure,^[10] which effectively suppressed the solubility of the active materials and consequently achieved an improved cycling lifetime of 500 h. Despite the effectiveness, the performance of the OEMs designed by the above strategies is

Q.-Q. Sun, H.-M. Xie
 National & Local United Engineering Laboratory for Power Battery
 Department of Chemistry
 Northeast Normal University
 Changchun, Jilin 130024, China
 E-mail: xiehm136@nenu.edu.cn

Q.-Q. Sun, J.-Y. Du, Z.-B. Zhuang, Z.-L. Xie, G. Huang, X.-B. Zhang
 State Key Laboratory of Rare Earth Resource Utilization
 Changchun Institute of Applied Chemistry
 Chinese Academy of Sciences
 Changchun 130022, China
 E-mail: ghuang@ciac.ac.cn; xbzhang@ciac.ac.cn

J.-Y. Du, Z.-L. Xie, G. Huang, X.-B. Zhang
 School of Applied Chemistry and Engineering
 University of Science and Technology of China
 Hefei 230026, China

T. Sun
 Institute of Quantum and Sustainable Technology
 School of Chemistry and Chemical Engineering
 Jiangsu University
 Zhenjiang 212013, China

The ORCID identification number(s) for the author(s) of this article can be found under <https://doi.org/10.1002/adma.202313388>

DOI: 10.1002/adma.202313388

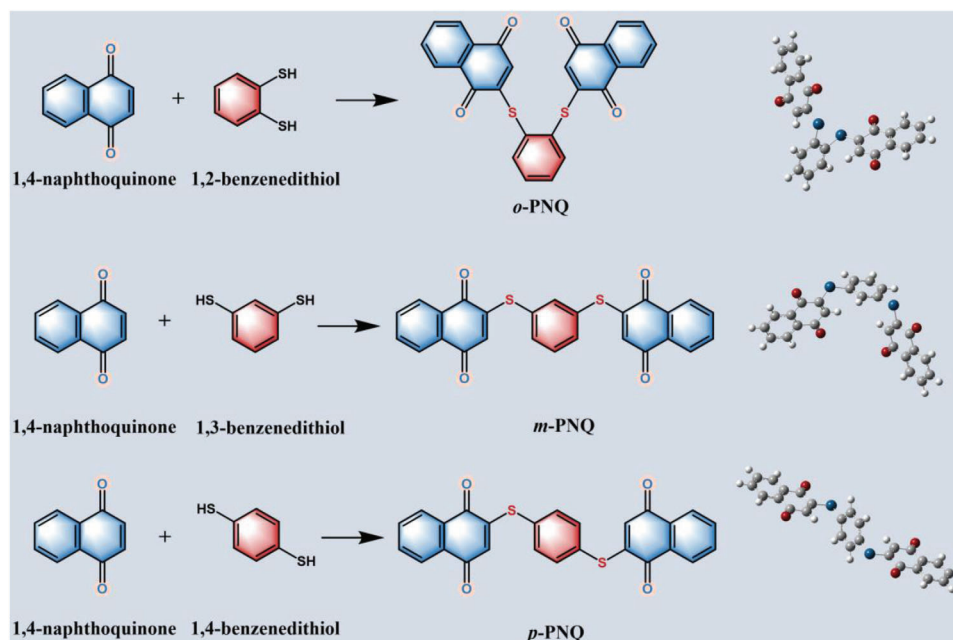


Figure 1. Schematic illustration of the synthesis of *o*-PNQ, *m*-PNQ, and *p*-PNQ.

still unsatisfactory.^[11–13] This can be ascribed to the introduction of inactive components and the enhancement of structural rigidity that make it difficult to obtain prolonged cycling lifetime and high specific capacity at the same time. In addition, most of the research on OEMs is at the primary level of molecular chemistry, which includes the atomic structure and related chemical bonding and also the design of functional groups to behave as the reaction sites. Nevertheless, the spatial structure is also an important feature of organic molecules in molecular chemistry, which inevitably has a significant impact on the Zn²⁺ ion storage performance. The neglect of the inherent spatial structure properties of OEMs has hindered their further performance improvement, not to mention the acquisition of high-performance zinc-organic batteries.

Small molecule carbonyl compounds with high electrochemical activity and abundant sources, as a type of OEMs, face the same dilemma of low achievable capacity and high solubility in the electrolyte.^[14,15] Designing carbonyl molecules with extended π -conjugated structure is also generally considered to be an effective approach to enhance the π -electron delocalization and reduce the solubility, thus optimizing the Zn²⁺ ion storage properties. However, the performance improvement by this kind of planar structure design through increasing the number of benzene rings has already reached the saturation point and would also bring a negative effect on reducing the theoretical specific capacities of carbonyl molecules. In terms of the neglect of the spatial structure properties of carbonyl compounds and the poor understanding of the molecular structure-electrochemical performance relationship, the construction of carbonyl compounds from the viewpoint of spatial structure design provides a promising path to realize high active group utilization and improved stability simultaneously.

Herein, we have ingeniously designed three S-linked quinone-derived isomers with adjustable spatial structures by regulating

the substituted position of S (Figure 1). Compared with the plane configuration of the conventional naphthoquinone derivatives, the introduction of the well-chosen S linkers makes the 2,2'-(1,2-phenylenedithio) bis(1,4-naphthoquinone) (*o*-PNQ), 2,2'-(1,3-phenylenedithio) bis(1,4-naphthoquinone) (*m*-PNQ), and 2,2'-(1,4-phenylenedithio) bis(1,4-naphthoquinone) (*p*-PNQ) (PNQs) possess nonplanar and partially conjugated structures, which are conducive to the high structure stability and redox unit independence with improved utilization of active sites. More importantly, the dissimilar spatial structures endow the designed PNQs with different zincophilic activity and redox kinetics. Benefiting from the smallest steric hindrance and the strongest electrochemical activity, the 2,2'-(1,4-phenylenedithio) bis(1,4-naphthoquinone) (*p*-PNQ) delivers a high reversible specific capacity of 279 mAh g⁻¹, an ultrafast rate capability of 167 mAh g⁻¹ at 100 A g⁻¹, and an excellent cycling life of 7000 cycles at 20 A g⁻¹. This work provides new guidance for the design of high-performance OEMs for promoting the real-world application of AZIBs for large-scale energy storage.

2. Results and Discussion

1,4-Naphthoquinone (1,4-NQ) was chosen as the basic structural unit for conducting our experiment due to its promising high electrochemical activity toward the Zn²⁺ ions. As shown in Figure S1 (Supporting Information), the 1,4-NQ exhibits one pair of redox peaks at 0.68 V/0.99 V in AZIBs and achieves a specific capacity of over 300 mAh g⁻¹ in the first cycle. Unfortunately, the 1,4-NQ experiences rapid capacity decay due to its high solubility in the electrolyte. Then, the traditional strategy of extending the π -conjugated structure was adopted to optimize the performance of OEMs.^[16,17] As an example, the naphthoquinone-derived 5,7,12,14-pentacenetetrone (PT) with an extended π -conjugated plane structure was designed here (inset in

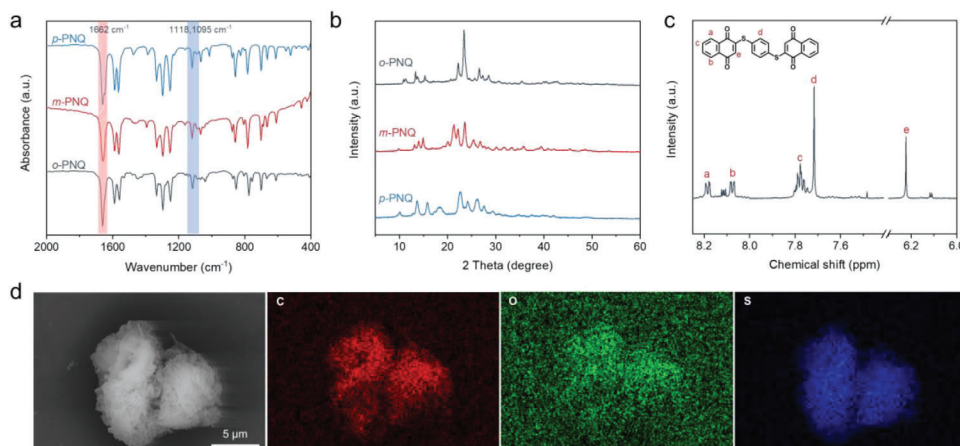


Figure 2. Characterizations of PNQs. a) Fourier transform infrared (FTIR) spectra and b) XRD patterns of PNQs; c) ^1H NMR and d) EDS mapping of *p*-PNQ.

Figure S2, Supporting Information). It can be seen from Figure S2a (Supporting Information) that the PT shows three pairs of redox peaks, indicating a multistep reaction occurs during the redox process. The voltage platforms in the discharge/charge curves are consistent with the CV results, and the PT delivers a specific capacity of 240 mAh g^{-1} in the first cycle (Figure S2b, Supporting Information). Obviously, the introduction of inactive benzene rings could slightly suppress the capacity decay but at the expense of the specific capacity of 1,4-NQ. Besides, the planar conformation of PT greatly decreases the intramolecular vibration and molecular flexibility, and this rigid structure also has a negative impact on the electrochemical reversibility, resulting in lower coulombic efficiencies. Therefore, it is crucial to consider the achievable capacity, structural stability, and also the ability to withstand the repeated storage/release of Zn^{2+} in the structural design of OEMs.

To realize this, three naphthoquinone-derived isomers with different spatial structures: *o*-PNQ, *m*-PNQ, and *p*-PNQ, were designed^[18] with the aim of improving the electrochemical activity of naphthoquinone while minimizing the introduction of inactive groups (Figure 1). The structures of the synthesized PNQs were firstly proved by different characterizations. In Figure 2a, the characteristic peak at 1662 cm^{-1} of the Fourier transform infrared (FTIR) spectra could be identified to the C=O groups, and the stretching vibration peaks around 1118 and 1095 cm^{-1} refer to the signal of C–S bonds, proving the successful formation of the thioether groups in PNQs. The remaining peaks belong to the vibrations of C=C and C–H bonds in 2-naphthyl. Figure 2b reveals the high crystallinity of the obtained PNQs, which is different from the traditional amorphous organic compounds and is beneficial to facilitate the electron transfer.^[19,20] The ^1H nuclear magnetic resonance (^1H NMR) spectrum of the *p*-PNQ was also collected to confirm its high purity (Figure 2c), which can be further supported by the EDS mapping (Figure 2d) and elemental analysis (Table S1, Supporting Information). For *o*-PNQ and *m*-PNQ, their purity has been verified by the ^1H NMR spectra (Figure S3, Supporting Information). Figures 2d and S4 (Supporting Information) give the morphology information of the PNQs with the shape of microspheres assembled by nanosheets/nanoplates.

The designed PNQ isomers with the same molecular formula but different spatial structures were then employed as cathode materials for AZIBs to establish a comprehensive understanding of the relationship between the spatial configuration and electrochemical performance. In Figure 3a, the CV curve of the *o*-PNQ shows two pairs of redox peaks at $0.94\text{ V}/0.78\text{ V}$ and $0.82\text{ V}/0.71\text{ V}$. Meanwhile, the *m*-PNQ and *p*-PNQ just exhibit one pair of redox peaks at $0.96\text{ V}/0.66\text{ V}$ and $0.91\text{ V}/0.71\text{ V}$, respectively. Obviously, the *p*-PNQ exhibits the smallest polarization. This is related to the different spatial structures of the three isomers, which will be detailedly discussed in the following part. In Figure 3b, the galvanostatic charge/discharge curves reveal that all PNQs only have one obvious charge/discharge plateau like the starting 1,4-NQ (Figure S1b, Supporting Information). This suggests that the incomplete conjugate structures of PNQs could keep the redox units relatively independent and consequently realize the high utilization of the active sites. Therefore, the *o*-PNQ, *m*-PNQ, and *p*-PNQ deliver high specific capacities of 259 , 263 , and 279 mAh g^{-1} at 0.05 A g^{-1} (Figure 3b), respectively, much larger than the reversible capacity of PT with a plane structure (Figure S2, Supporting Information). Clearly, the reasonable introduction of the inactive components to adjust the spatial structure of OEMs could ensure the realization of high specific capacity, which has never been achieved by the plane structure design. To minimize the interference caused by the conductive agent, a purer comparison of PNQs was further conducted. The proportion of the conductive agent was reduced to 10%, while the active material was increased to 80% for the electrode preparation (referred to as *o*-PNQ-811, *m*-PNQ-811, and *p*-PNQ-811). The *o*-PNQ-811, *m*-PNQ-811, and *p*-PNQ-811 exhibit specific capacities of 178 , 205 , and 258 mAh g^{-1} at 0.02 A g^{-1} , respectively (Figure S5, Supporting Information). This reveals that the spatial structures of PNQs have a significant effect on their performance release, and the centrosymmetric structure of naphthoquinones on the benzene rings of *p*-PNQ make it stand out among the designed PNQs. As indicated in Figure 3c, a superb rate capability of *p*-PNQ is also achieved with stable reversible capacities of 200 , 197 , 194 , 193 , 193 , 182 , and 167 mAh g^{-1} at 1 , 2 , 5 , 10 , 20 , 50 , and 100 A g^{-1} , respectively. When the current density immediately drops back to 1 A g^{-1} , the specific capacity of *p*-PNQ is able to recover to

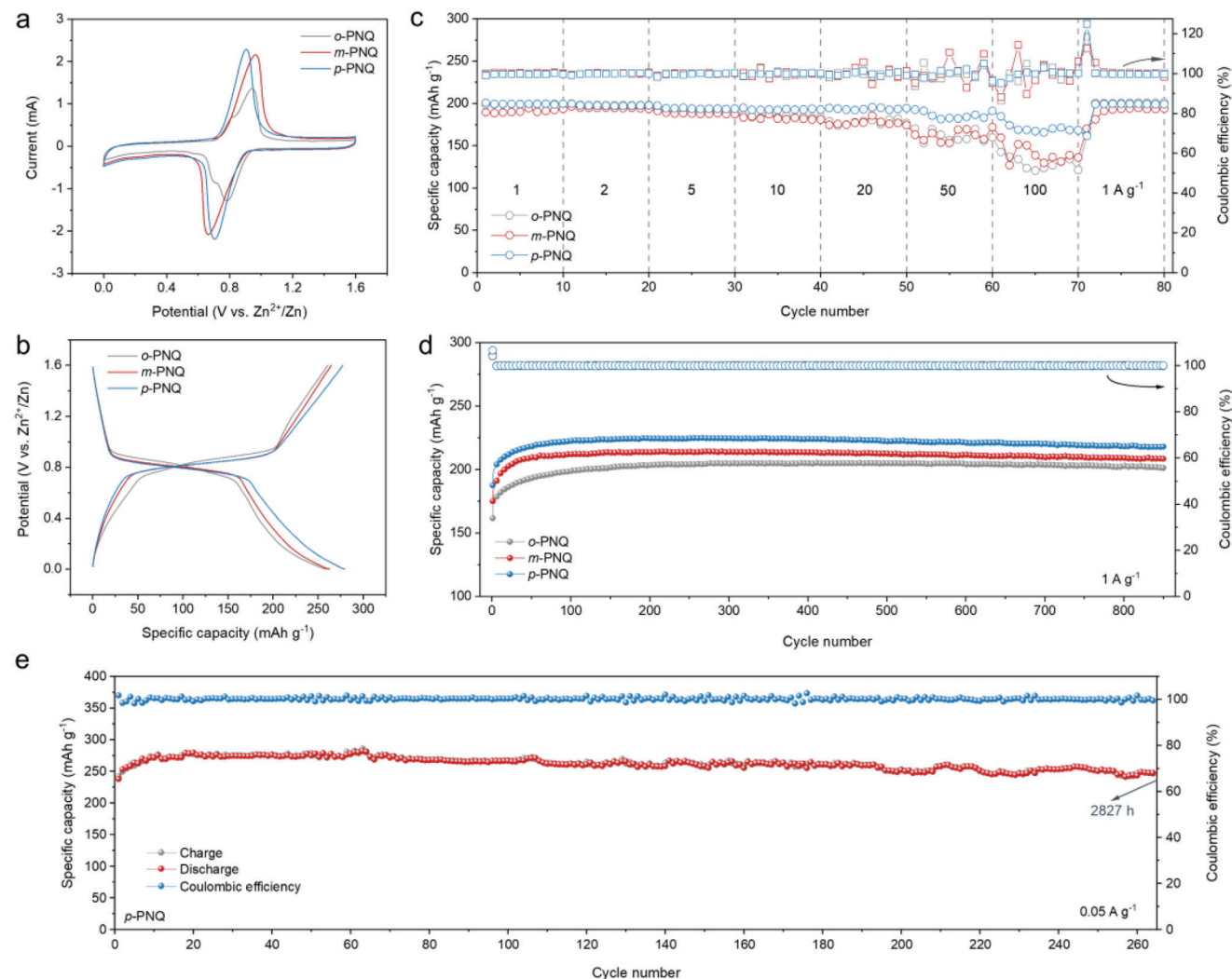


Figure 3. Electrochemical performance of PNQs. a) CV curves at 0.5 mV s^{-1} , b) discharge/charge curves at 0.05 A g^{-1} , c) rate performance, and d) cycling performance at 1 A g^{-1} ; e) cycling performance of p -PNQ at 0.05 A g^{-1} .

the initial value. Similarly, the o -PNQ and m -PNQ also present excellent electrochemical reversibility and rate performance but always maintain a trend of p -PNQ > m -PNQ > o -PNQ in terms of capacity. Even at a high mass loading of 8 mg cm^{-2} , the p -PNQ could still deliver high capacities of 196, 188, 177, 169, and 151 mAh g^{-1} at 1, 2, 5, 10, and 20 A g^{-1} (Figure S6, Supporting Information).

Considering that the partial conjugation of the nonplanar PNQs could not only realize the independence of the active functional groups but also facilitate the expansion of quinone molecular structures with the benefit of alleviating the dissolution issue in the aqueous solution, the long-term cycling stability of PNQs was then studied. As shown in Figure 3d, the o -PNQ, m -PNQ, and p -PNQ exhibit stable cycling performance at 1 A g^{-1} with the specific capacities of 201, 208, and 218 mAh g^{-1} after 850 cycles, respectively, revealing that our spatial structural design enables the three naphthoquinone-derived materials to obtain significantly enhanced structural stability. Furthermore, the high electrochemical stability of the PNQs has also been demon-

strated in a low current density of 0.05 A g^{-1} . In Figure 3e, the p -PNQ delivers a capacity retention of 90% after 2827 h cycling at 0.05 A g^{-1} , which is better than those of the o -PNQ and m -PNQ ($\approx 2300 \text{ h}$, Figure S7, Supporting Information). This can be ascribed to the centrosymmetric molecular conformation of the p -PNQ that helps to regulate the inhomogeneous deformation stress within the crystal during the repeated discharge/charge processes.^[21] Even increased the current density to 20 A g^{-1} , the p -PNQ could still display a cycling lifetime of over 7000 cycles with a capacity retention of 93% (Figure S8, Supporting Information). Besides, the p -PNQ could maintain a large reversible capacity of 153 mAh g^{-1} after 800 cycles (capacity retention ratio of 94%, Figure S9, Supporting Information) at a rigorously high current density of 100 A g^{-1} . The SEM images of the p -PNQ electrodes before and after the cycling test clear show that the p -PNQ could well maintain its initial morphology without obvious structural change after the cycling, signifying its high structure stability (Figure S10, Supporting Information). Similarly, the o -PNQ and m -PNQ also achieve stable cycling at 20 A g^{-1} except with low

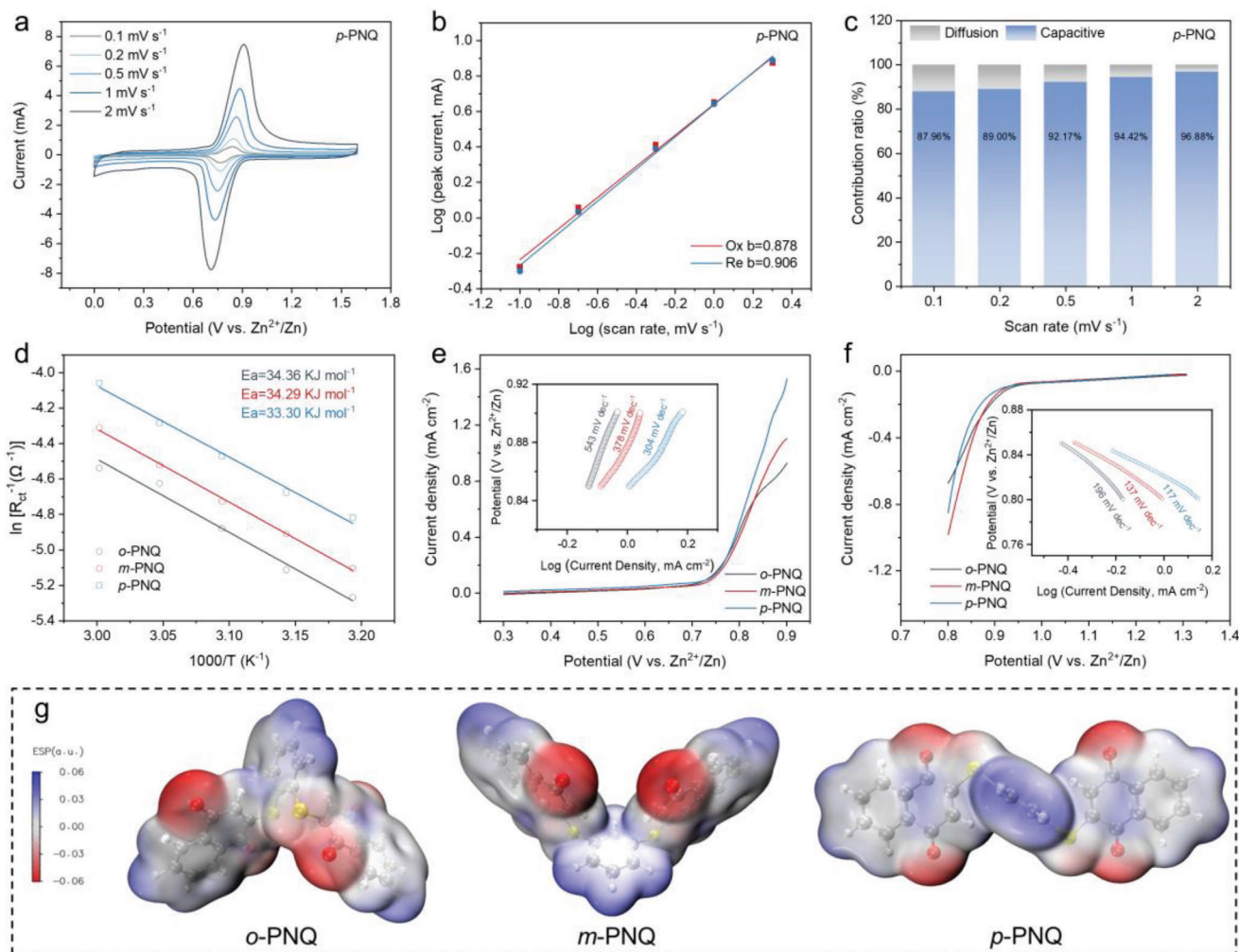


Figure 4. Reaction kinetics analysis of PNQs. a) CV curves of *p*-PNQ at different scan rates. b) Power law dependence of the measured current on scan rate at corresponding peak potentials of *p*-PNQ. c) Contribution ratios of the capacitive charge storage of *p*-PNQ at different scan rates. d) The Arrhenius plots of $\ln(R_{ct}^{-1})$ versus $1000/T$; LSV curves for the e) oxidation and f) reduction processes and the corresponding calculated Tafel slopes; g) electrostatic potential (ESP) mappings of PNQs.

capacities. These results confirm that besides the high achievable capacity and rate capability, the rational spatial structure design could also enable the OEMs to fulfill long-term cycling stability, especially, the *p*-PNQ with a central symmetry structure delivers the most excellent overall performance. It should be mentioned that the performance of *p*-PNQ achieved here is superior to the previously reported OEMs in terms of the rate capability, cycling lifetime, capacity degradation rate, and energy density (Figure S11 and Table S2, Supporting Information), especially to the carbonyl compounds with similar structures (Table S3, Supporting Information).^[10,12,22–33] Additionally, a set of electrochemical performance data of the batteries assembled by three different synthetic batches of *p*-PNQ has been provided to demonstrate the reproducibility of electrochemical data (Figure S12, Supporting Information).

After validating the superior Zn^{2+} ion storage properties of the PNQs, their reaction kinetics was investigated by performing CV test at different scan rates (Figures 4a and S13a,d, Supporting

Information). The relationship between the peak current (i) and sweep rate (ν) in CV curves can be described as: $i = a\nu^b$ (where a and b are adjustable parameters). The b -value close to 0.5 indicates the diffusion-controlled process, and 1.0 corresponds to the capacitance-dominated process. As calculated in Figure 4b, the b -values of the cathodic and anodic peaks for *p*-PNQ are 0.878 and 0.906, indicating that the energy storage process of *p*-PNQ is capacitive-dominant. Furthermore, the capacitive contribution of *p*-PNQ boosts from 87.96% to 96.88% with the increase of scan rate from 0.1 to 2 $mV s^{-1}$ (Figure 4c), proving the fast redox kinetics of *p*-PNQ. Likewise, the *o*-PNQ and *m*-PNQ also present high b -values with a gradually increased capacitance-dominant Zn^{2+} storage process (*o*-PNQ < *m*-PNQ < *p*-PNQ, Figure S13, Supporting Information). From the above analysis, it is clear that all the PNQs have fast reaction kinetics prevailed by the capacitive process, which is consistent with their excellent rate performance. The specific differences in the kinetics among the three isomers can be ascribed to their structural diversity that affects the

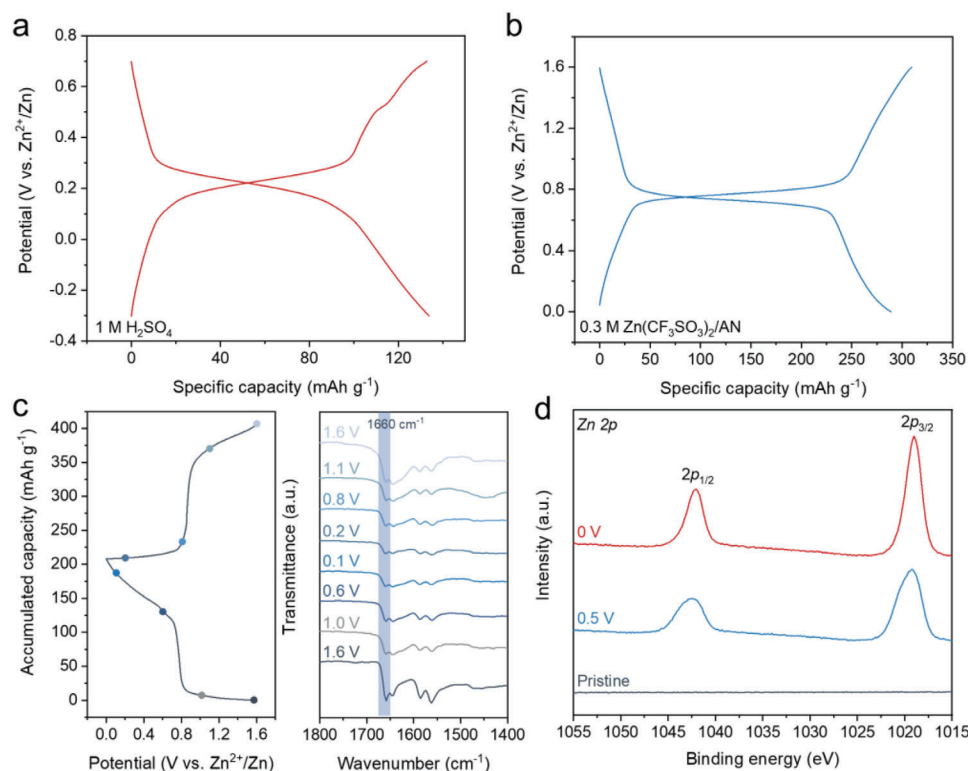


Figure 5. Energy storage mechanism analysis of *p*-PNQ. Discharge/charge curves in a) 1 M H₂SO₄ and b) 0.3 M Zn(CF₃SO₃)₂/AN; c) ex situ Fourier transform infrared (FTIR) and d) ex situ XPS spectra at different states.

spatial hindrance and electron distribution within the molecule and consequently results in different zincophilic activities and reaction kinetics.^[34]

In order to deeply explore the impact of the spatial structures of PNQs on the energy storage process, a more detailed reaction kinetics analysis was carried out. The electrochemical impedance spectroscopy (EIS) measurement of PNQs at different temperatures was first conducted.^[35] As shown in Figure S14 (Supporting Information), the *p*-PNQ displays the smallest charge transfer impedance (R_{ct}) across all test temperatures, meaning the *p*-PNQ has the highest electrical conductivity compared to the *o*-PNQ and *m*-PNQ. The centrosymmetric structure could endow the *p*-PNQ with the smallest dipole moment, thus boosting the intramolecular electron transfer.^[34] In addition, the *p*-PNQ also exhibits the maximum slopes in the low frequency region, implying the minimum Warburg impedance with the fastest mass transfer process and thus consisting with the rapid reaction kinetics of *p*-PNQ. At the same time, the activation energy (E_a) of the three isomers was calculated based on the Arrhenius equation. The E_a of *o*-PNQ, *m*-PNQ, and *p*-PNQ are 34.36, 34.29, and 33.30 KJ mol⁻¹ (Figure 4d), respectively. The minimum E_a value of the *p*-PNQ endows it with the fastest redox kinetics and accordingly the best rate performance. Figure 4e,f gives the Tafel slopes of the PNQs. The Tafel slopes calculated from the oxidation peaks are 543, 378, and 304 mV dec⁻¹ for the *o*-PNQ, *m*-PNQ, and *p*-PNQ, respectively. And the corresponding Tafel slopes are 196, 137, and 117 mV dec⁻¹ for the *o*-PNQ, *m*-PNQ, and *p*-PNQ in the reduction process. The high electrical conductivity and low Warburg impedance, E_a , and Tafel slopes demonstrate that

the *p*-PNQ possesses the best electrochemical activity toward Zn²⁺.^[36]

To delve into the fundamental factors contributing to the performance differences, a more in-depth study on the spatial structures of the three isomers was conducted. Considering the presence of nonrotatable C=C bonds in the PNQs, both *cis*- and *trans*-configurations would exist. To this end, the dominant configurations of PNQs have been well deduced with the sufficient support of theoretical calculations, which are *trans-o*-PNQ, *cis-m*-PNQ, and *trans-p*-PNQ, respectively (Figure S15, Supporting Information). Also, it is clearly that the optimized geometry of the two naphthoquinone-based planes for the *trans-p*-PNQ possesses a dihedral angle close to 180° (Figure S16, Supporting Information). This optimal dihedral angle could enable the *p*-PNQ with the smallest spatial hindrance for Zn²⁺ ion storage when compared with the *o*-PNQ and *m*-PNQ, and consequently, conducive to the full utilization of active functional groups with high reversible capacities. Furthermore, the quantum chemical properties of the PNQs were detailedly studied to explore the internal factors contributing to their performance differences. Since the binding of PNQs with Zn²⁺ can be considered as an electrophilic reaction, so the areas with higher electronegativity are more attractive to behave as the reaction sites. In view of this, the molecular electrostatic potential (ESP) of the PNQs was calculated to predict the exposure of the active sites (Figure 4g).^[37] According to the ESP mapping results, the regions near the carbonyl groups of PNQs exhibit more negative ESP values and are considered to be highly reactive sites. Compared with the *o*-PNQ and *m*-PNQ, the *p*-PNQ displays the most dispersed distribution of

the electronegativity regions, providing sufficient spaces for the full and efficient binding of Zn^{2+} . Besides, the molecular orbital energy levels of PNQs were also calculated to check the spatial structure induced electronic structure differences. As shown in Figure S17 (Supporting Information), the LUMO orbitals of all the three PNQs are concentrated on the naphthoquinone moieties. Considering the LUMO orbital has strong electron affinity and possesses the property to act as electron acceptors, the concentration of LUMO orbitals on the naphthoquinone moieties proves their independence of redox reactions. For *p*-PNQ, it possesses a well dispersed LUMO orbital, indicating that there is less interference between the active sites and thus facilitating the rapid binding/release of Zn^{2+} . The physical characteristics of PNQs also could directly affect their electrochemical performance. From Figure S18a (Supporting Information), we can see that only *p*-PNQ with the *trans*-configuration is centrosymmetric with a dipole-moment of 0 Debye, which can trigger strong intramolecular electron transfer. After this, ultraviolet visible (UV-Vis) measurement was performed to calculate the optical energy gaps (E_g) of PNQs, which follow the sequence of *o*-PNQ (2.43 eV) > *m*-PNQ (2.38 eV) > *p*-PNQ (2.32 eV) (Figure S18b, Supporting Information). With the lowest E_g , the *p*-PNQ is expected to endow better charge transfer ability and accordingly stimulate redox reaction with a lower kinetics threshold.^[31] In sum, the *p*-PNQ with the optimal dihedral angle, highly dispersed distributions of electronegativity regions and LUMO orbital, and lowest optical energy gap makes it deliver the best Zn^{2+} ion storage properties. For *o*-PNQ, its largest steric hindrance generated by the proximity of naphthoquinones on the benzene rings makes the redox process experience a continuous two-step reaction (CV curves in Figure 3a), which is different from *m*-PNQ and *p*-PNQ and also in agreement with its lowest achievable capacity.

Since the existence of H^+ in the 2 M $\text{Zn}(\text{CF}_3\text{SO}_3)_2$ aqueous electrolyte, the *p*-PNQ was selected as the representative to study its detailed ion storage mechanism. In Figure 5a, the *p*-PNQ delivers a specific capacity of 133 mAh g^{-1} at 0.05 A g^{-1} in the 1 M H_2SO_4 electrolyte without Zn^{2+} ions, suggesting the available H^+ -storage activity of *p*-PNQ. When operated in the 0.03 M $\text{Zn}(\text{CF}_3\text{SO}_3)_2/\text{AN}$ electrolyte, the *p*-PNQ could give a specific capacity of 289 mAh g^{-1} (Figure 5b), which is almost the same as that in 2 M $\text{Zn}(\text{CF}_3\text{SO}_3)_2$ electrolyte, manifesting the strong Zn^{2+} -storage activity of *p*-PNQ. Additionally, the *p*-PNQ also exhibits high cycle stability of over 2700 h with a capacity retention rate of 89% at 0.05 A g^{-1} in the organic electrolyte (Figure S19, Supporting Information), which is comparable to the stability in the aqueous electrolyte (Figure 3e). Considering the relatively low H^+ concentration in the 2 M $\text{Zn}(\text{CF}_3\text{SO}_3)_2$ electrolyte (pH = 3.7) and the higher Zn^{2+} -storage activity of *p*-PNQ, it can be concluded that the ion storage mechanism of *p*-PNQ in the aqueous electrolyte is dominated by the Zn^{2+} -storage with the partial involvement of H^+ . To support this, ex situ FTIR spectra of *p*-PNQ at different states were collected. As shown in Figure 5c, the C=O peak around 1660 cm^{-1} gradually weakens with the deepening of the discharge process and recovers step by step in the following re-charging process, demonstrating the high reversibility of the enolization associated ion storage/release. Additionally, as shown in Figure S20 (Supporting Information), the in situ Raman spectra also accurately reveal the evolution process of C=O in *p*-PNQ during the discharge/charge process. For confirming the Zn^{2+} in-

volved energy storage mechanism, the ex XPS measurement was performed. It can be seen from Figure 5d that there are strong peaks in the Zn 2p region for the *p*-PNQ discharged to 0.5 V, and the intensity of the Zn peaks strengthens with the increase of discharge depth. In the O 1s XPS spectra, the characteristic peak of the C=O group (531 eV) disappears, and a new C–O–Zn peak (530.5 eV) appears for the fully discharged *p*-PNQ (Figure S21, Supporting Information), verifying the coordination of Zn^{2+} with C–O[−] during the discharge process.

3. Conclusion

In conclusion, the PNQ isomers with controllable spatial structures have been synthesized by a reasonable molecular engineering strategy. On the one hand, the presence of C–S–C bonds endows the PNQs with flexible nonplanar structures to accommodate the inhomogeneous deformation stress within the crystal during cycling, boosting the electrochemical stability. On the other hand, the partial conjugation structure makes the redox units of PNQs relatively independent and consequently realizes the high utilization of the active sites. Importantly, the relationship between the spatial structure and electrochemical performance has been established through the detailed investigation of *o*-PNQ, *m*-PNQ, and *p*-PNQ. Among them, the *p*-PNQ with the smallest steric hindrance and the most independent redox of active sites enables the *p*-PNQ||Zn cell to display a high specific of 279 mAh g^{-1} , an ultrarapid rate performance (167 mAh g^{-1} at 100 A g^{-1}), and a long lifetime over 2800 h. This work deepens our understanding of the correlation between the stereochemical structure and electrochemical performance and provides new guidance for the spatial structural design of high-performance OEMs.

Supporting Information

Supporting Information is available from the Wiley Online Library or from the author.

Acknowledgements

Q.Q.S., J.Y.D., and T. S. contributed equally to this work. This work was financially supported by the National Key R&D Program of China (2020YFE0204500), National Natural Science Foundation of China (52171194 and 52071311), Jilin Province Science and Technology Development Plan Funding Project (Grant YDZJ202301ZYTS545), Youth Innovation Promotion Association CAS (Grant 2020230), and National Natural Science Foundation of China Outstanding Youth Science Foundation of China (Overseas).

Conflict of Interest

The authors declare no conflict of interest.

Data Availability Statement

The data that support the findings of this study are available from the corresponding author upon reasonable request.

Keywords

carbonyl compound materials, organic electrodes, spatial structure, Zn-organic batteries

Received: December 9, 2023

Revised: January 27, 2024

Published online:

- [1] L. Ma, M. A. Schroeder, O. Borodin, T. P. Pollard, M. S. Ding, C. Wang, K. Xu, *Nat. Energy* **2020**, *5*, 743.
- [2] X. Jia, C. Liu, Z. G. Neale, J. Yang, G. Cao, *Chem. Rev.* **2020**, *120*, 7795.
- [3] P. Yu, Y. Zeng, H. Zhang, M. Yu, Y. Tong, X. Lu, *Small* **2019**, *15*, 1804760.
- [4] X. Yun, Y. Chen, P. Xiao, C. Zheng, *J. Electrochem.* **2022**, *28*, 2219004.
- [5] Y. Lu, Q. Zhang, L. Li, Z. Niu, J. Chen, *Chem* **2018**, *4*, 2786.
- [6] Y. Chen, K. Fan, Y. Gao, C. Wang, *Adv. Mater.* **2022**, *34*, 2200662.
- [7] Y. Lu, J. Chen, *Nat. Rev. Chem.* **2020**, *4*, 127.
- [8] Y. Liang, Y. Yao, *Joule* **2018**, *2*, 1690.
- [9] J. Huang, X. Dong, Z. Guo, Y. Ma, Y. Wang, Y. Wang, *J. Electrochem.* **2020**, *26*, 486.
- [10] T. Sun, Z. Yi, W. Zhang, Q. Nian, H. J. Fan, Z. Tao, *Adv. Funct. Mater.* **2023**, *33*, 2306675.
- [11] Z. Lin, H.-Y. Shi, L. Lin, X. Yang, W. Wu, X. Sun, *Nat. Commun.* **2021**, *12*, 4424.
- [12] T. Sun, W. Zhang, Z. Zha, M. Cheng, D. Li, Z. Tao, *Energy Storage Mater.* **2023**, *59*, 102778.
- [13] H. Cui, T. Wang, Z. Huang, G. Liang, Z. Chen, A. Chen, D. Wang, Q. Yang, H. Hong, J. Fan, C. Zhi, *Angew. Chem., Int. Ed.* **2022**, *61*, 202203453.
- [14] Z. Guo, Y. Ma, X. Dong, J. Huang, Y. Wang, Y. Xia, *Angew. Chem., Int. Ed.* **2018**, *57*, 11737.
- [15] Q. Zhao, W. Huang, Z. Luo, L. Liu, Y. Lu, Y. Li, L. Li, J. Hu, H. Ma, J. Chen, *Sci. Adv.* **2018**, *4*, eaao1761.
- [16] M. Yu, R. Dong, X. Feng, *J. Am. Chem. Soc.* **2020**, *142*, 12903.
- [17] C. Wang, Y. Xu, Y. Fang, M. Zhou, L. Liang, S. Singh, H. Zhao, A. Schober, Y. Lei, *J. Am. Chem. Soc.* **2015**, *137*, 3124.
- [18] B. Zhao, Y. Si, W. Guo, Y. Fu, *Adv. Funct. Mater.* **2022**, *32*, 2112225.
- [19] Y. C. Ye, L. Chen, X. M. Chen, C. Y. Ma, B. H. Lv, J. Y. Wang, W. D. Dou, C. Zhang, T. L. Ma, J. X. Tang, *Adv. Funct. Mater.* **2023**, 2310136.
- [20] S. Li, J. Shang, M. Li, M. Xu, F. Zeng, H. Yin, Y. Tang, C. Han, H.-M. Cheng, *Adv. Mater.* **2023**, *35*, 2207115.
- [21] Y. Wang, W. Zhang, J. Yang, Y. Gong, J. Zhang, M. Fang, Q.-H. Yang, Z. Li, *Matter* **2022**, *5*, 4467.
- [22] Y. Wang, C. Wang, Z. Ni, Y. Gu, B. Wang, Z. Guo, Z. Wang, D. Bin, J. Ma, Y. Wang, *Adv. Mater.* **2020**, *32*, 2000338.
- [23] F. Ye, Q. Liu, H. Dong, K. Guan, Z. Chen, N. Ju, L. Hu, *Angew. Chem., Int. Ed.* **2022**, *61*, 202214244.
- [24] X. Wang, J. Xiao, W. Tang, *Adv. Funct. Mater.* **2021**, *32*, 2108225.
- [25] X. Wang, J. Tang, W. Tang, *Adv. Funct. Mater.* **2022**, *32*, 2200517.
- [26] H.-Y. Shi, Y.-J. Ye, K. Liu, Y. Song, X. Sun, *Angew. Chem., Int. Ed.* **2018**, *57*, 16359.
- [27] N. Wang, Z. Guo, Z. Ni, J. Xu, X. Qiu, J. Ma, P. Wei, Y. Wang, *Angew. Chem., Int. Ed.* **2021**, *60*, 20826.
- [28] L. Yan, Q. Zhu, Y. Qi, J. Xu, Y. Peng, J. Shu, J. Ma, Y. Wang, *Angew. Chem., Int. Ed.* **2022**, *61*, 202211107.
- [29] H. Zhang, Y. Fang, F. Yang, X. Liu, X. Lu, *Energy Environ. Sci.* **2020**, *13*, 2515.
- [30] T. Sun, Z. J. Li, Y. F. Zhi, Y. J. Huang, H. J. Fan, Q. Zhang, *Adv. Funct. Mater.* **2021**, *31*, 2010049.
- [31] L. Yan, Y. Zhang, Z. Ni, Y. Zhang, J. Xu, T. Kong, J. Huang, W. Li, J. Ma, Y. Wang, *J. Am. Chem. Soc.* **2021**, *143*, 15369.
- [32] M. Tang, Q. Zhu, P. Hu, L. Jiang, R. Liu, J. Wang, L. Cheng, X. Zhang, W. Chen, H. Wang, *Adv. Funct. Mater.* **2021**, *31*, 2102011.
- [33] K. W. Nam, H. Kim, Y. Beldjoudi, T.-W. Kwon, D. J. Kim, J. F. Stoddart, *J. Am. Chem. Soc.* **2020**, *142*, 2541.
- [34] Z. Song, L. Miao, H. Duan, L. Ruhlmann, Y. Lv, D. Zhu, L. Li, L. Gan, M. Liu, *Angew. Chem., Int. Ed.* **2022**, *61*, 202208821.
- [35] N. Wang, R. Zhou, H. Li, Z. Zheng, W. Song, T. Xin, M. Hu, J. Liu, *ACS Energy Lett.* **2021**, *6*, 1141.
- [36] L. Ma, G. Zhu, Z. Wang, A. Zhu, K. Wu, B. Peng, J. Xu, D. Wang, Z. Jin, *Nano Lett.* **2023**, *23*, 5272.
- [37] L. Liu, L. Miao, L. Li, F. Li, Y. Lu, Z. Shang, J. Chen, *J. Phys. Chem. Lett.* **2018**, *9*, 3573.